Unknown Input Observers for Simultaneous Estimation of Vehicle Dynamics and Driver Torque: Theoretical Design and Hardware Experiments

Tran Anh-Tu Nguyen, Thierry-Marie Guerra, Chouki Sentouh, Hui Zhang

Unknown Input Observers for Simultaneous Estimation of Vehicle Dynamics and Driver Torque: Theoretical Design and Hardware Experiments

Article *in* IEEE/ASME Transactions on Mechatronics · December 2019

DOI: 10.1109/TMECH.2019.2933744

CITATIONS
47

READS
741

4 authors, including:

Anh-Tu Nguyen
Université Polytechnique Hauts-de-France
140 PUBLICATIONS **2,084** CITATIONS
SEE PROFILE

Thierry-Marie Guerra
Université Polytechnique Hauts-de-France
349 PUBLICATIONS **9,873** CITATIONS
SEE PROFILE

Chouki Sentouh
LAMIH UMR CNRS 8201 Hauts-de-France Polytechnic University
114 PUBLICATIONS **2,057** CITATIONS
SEE PROFILE

Unknown Input Observers for Simultaneous Estimation of Vehicle Dynamics and Driver Torque: Theoretical Design and Hardware Experiments

Anh-Tu Nguyen*, *Member, IEEE*, Thierry-Marie Guerra, Chouki Sentouh, *Member, IEEE*, and Hui Zhang, *Senior Member, IEEE*

***Abstract*—This paper investigates a new observer design method to estimate *simultaneously* both the vehicle dynamics and the unknown driver's torque. To take into account the time-varying nature of the longitudinal speed, the vehicle system is transformed into a polytopic linear parameter-varying (LPV) model with a reduced level of numerical complexity. Based on Lyapunov stability arguments, we prove that the estimation errors of the system state and of the unknown input (UI) are norm-bounded, which can be made *arbitrarily* small by minimizing a guaranteed $\mathcal{L}_\infty-$gain performance. The design of the LPV unknown input observer is reformulated as an LMI-based optimization which can be effectively solved via semidefinite programming. Extensive hardware experiments are carried out under various driving test scenarios to confirm the effectiveness of the proposed observer design. In particular, a comparative study is performed with a widely adopted observer to emphasize the practical interests of the new estimation solution.**

***Index Terms*—Vehicle dynamics, sideslip angle estimation, torque estimation, driver steering intervention, unknown input observer, $\mathcal{L}_\infty$ observer design.**

I. Introduction

A raising number of road accidents has greatly motivated the research and development on intelligent vehicles (IVs) to improve the ride safety and comfort [1]–[4]. As an essential part of IVs, online driver-vehicle monitoring and active safety control systems have gained increasing interests worldwide [4]–[7]. Real-time information of the vehicle dynamics and the driver-related variables is crucial to develop such feedback control and monitoring systems. Unfortunately, the onboard vehicle sensors are in general too expensive for commercial automotive applications [8], [9]. Moreover, in many specific contexts, the human driver variables cannot be directly measured by physical sensors [7]. Hence, estimation algorithms must be developed in these situations to reconstruct driver-vehicle variables with only measurements of low-cost sensors.

Due to its usefulness in many active safety applications and the prohibitive cost, the sideslip angle estimation has attracted considerable research efforts [8], [10]–[12]. General speaking, the sideslip angle estimation algorithms can be classified into three categories. First, the kinematic model-based methods [13], [14] rely on a simple vehicle model. Without requiring vehicle or tire friction parameters, these methods strongly depend on the sensor information, which can lead to the drift phenomena induced by bias errors [8]. Second, the dynamic model-based methods using Kalman filters [15]–[17] or robust observers [8], [18], [19] can overcome this major drawback. However, these methods usually require an accurate information on the vehicle parameters and tire-road conditions, especially for driving situations with high lateral acceleration [14]. Third, fusion-data-based methods have been proposed to exploit the advantages of the two above categories [10], [20], [21]. Note that these methods can introduce excessive costs and complexity to the vehicle design [14].

Model-based unknown input (UI) observers have been also proposed to estimate the vehicle dynamics together with UIs related to the vehicle-road characteristics. Based on a gradient descent algorithm, the authors in [12] proposed an UI observer to estimate the sideslip angle and the road friction. An algebraic-based UI observer was developed in [22] to reconstruct the lateral speed on an unknown banked road. Using the mean value theorem, a nonlinear observer was proposed in [23] to estimate the vehicle dynamics. Then, the unknown normal tire forces were recovered with a dynamic model inversion technique. Note that for simplicity, a constant vehicle speed was considered for observer design in most of existing works. Unfortunately, this strong assumption can lead to a poor estimation performance under various driving situations [8], [11]. The LPV unknown input observer, recently proposed in [24], can be used to overcome this drawback. However, this algebraic UI decoupling method and numerous related designs require a differentiation of the measured output for UI estimation, leading to a major practical issue [22]. Being able to avoid the above issues, the novel fuzzy UI observer in [11] can be used to estimate both the sideslip angle and the unknown steering angle of autonomous vehicles. This UI observer may induce practical difficulties for real-time purposes due to its important number of subsystems for fuzzy representation and a conservative Lipschitz-like assumption.

Despite of an extensive literature, UI observer designs for a *simultaneous* estimation of the sideslip angle and the human steering torque have not been well addressed. Nevertheless, such an estimation framework is crucial for many IVs appli-

This work is supported by the French Ministry of Higher Education and Research, the National Center for Scientific Research (CNRS), the Nord-Pas-de-Calais Region under the project ELSAT 2020. The work of Hui Zhang was supported by the National Natural Science Foundation of China under Grants U1664257 and U1864201.

A.-T. Nguyen, T.-M. Guerra and C. Sentouh are with the Université Polytechnique Hauts-de-France, laboratory LAMIH CNRS UMR 8201, F-59313 Valenciennes, France.

Hui Zhang is with the School of Transportation Science and Engineering, Beihang University, Beijing, China.

*Corresponding author (e-mail: nguyen.trananhtu@gmail.com).

cations, especially shared driving control [25], [26], or take-over control process [7], [27]. In these control situations, the driver torque is *jointly* applied to the steering wheel with an assistive torque from a driving assistance system to control the vehicle [9]. Hence, the human driver torque cannot be always measured by a torque sensor due to the driver-automation coupled input [7]. Designing an UI observer to reconstruct the driver torque is crucial to detect the human intervention in the driving process, thus to improve the shared control performance [26]. Surprisingly, very few works related to this topic can be found in the open literature. Using the dynamics of a steering wheel actuation system, the authors in [7] developed a nonlinear disturbance observer for the driver torque estimation. An $\mathcal{H}_\infty/\mathcal{H}_2$ proportional multi-integral (PMI) observer was used in [28] to estimate the driver torque from the dynamics of an electric power steering system. Remark that the vehicle dynamics, especially the sideslip angle, cannot be reconstructed with the observers in [7], [28]. The driver-vehicle estimation objective can be achieved with the UI observer in [29]. Exploiting the generalized design of PMI observers [30] for T-S fuzzy systems [31], this UI observer was designed while further taking into account the $\mathcal{D}-$stability constraints to improve the estimation performance. Note that for the observer designs in [7], [28]–[30], the UIs must be of *polynomial* form. This assumption is not always compatible with the driver torque signal in IVs applications [28].

This paper investigates a new UI observer design to estimate simultaneously the vehicle dynamics and the driver torque. The particular features of this cost-effective estimation solution can be summarized as follows.

1) In contrast to UI decoupling approaches [22], [24], [32], no differentiation of the measured output and/or the time-varying parameters are needed for the UI reconstruction. In addition, no matching conditions are explicitly imposed on the UIs as in [11], [22], [30] and numerous related references. Moreover, no *a priori* knowledge on the UIs is required as for the design of PMI observers [29], [30], [33]. Note that to improve the estimation performance, the order of PMI observers may be significantly larger than that of the plant systems, inducing complexities/difficulties for practical uses.
2) The proposed LPV observer enables *arbitrarily* small estimation errors by minimizing an $\mathcal{L}_\infty-$gain. Using Lyapunov-based arguments, the estimation performance is theoretically guaranteed. The observer design is recast as a linear matrix inequality (LMI) based optimization problem, which is efficiently solved with semidefinite programming [34]. Moreover, to reduce the conservatism, the information of both vehicle speed and acceleration is exploited in the observer design using a parameter-dependent Lyapunov function involving a slack variable.
3) The effectiveness of the new method is thoroughly verified through hardware experiments with an interactive driving simulator under various driving test conditions. Especially, a comparative study is performed with the widely adopted PMI observer design to emphasize the interests of the proposed estimation solution.

This paper extends our preliminary results in [19]. It provides additional theoretical results to further reduce the complexity and the conservatism of the design conditions through a new treatment of the parameter-dependent Lyapunov matrix. In particular, we include extensive experimental results and a comparative study with a PMI observer. The paper is organized as follows. Section II recalls the vehicle modeling and describes the observer problem. The vehicle system is transformed into a tractable LPV model for observer design in Section III. In Section IV, the new LMI-based observer design is first detailed for state estimation. Then, a method to reconstruct the UI is presented. The interests of the proposed method is experimentally demonstrated in Section V. Section VI provides some concluding remarks.

Notation. Ω_N denotes the set of numbers $\{1, 2, \ldots, N\}$. I denotes the identity matrix of appropriate dimension. For a matrix X, $X^\top$ indicates its transpose. For any square matrix X, $X \succ 0$ indicates a positive definite matrix, $\mathrm{He}X = X + X^\top$, and $\lambda_{\min}(X)$ (respectively $\lambda_{\max}(X)$) denotes the minimal (respectively maximal) eigenvalue of X. For a vector $\mathbf{x} \in \mathbb{R}^n$, we denote its 2-norm as $\|\mathbf{x}\| = \sqrt{\mathbf{x}^\top \mathbf{x}}$. For any bounded function $f(\cdot) : \mathbb{R} \to \mathbb{R}^n$, its $\mathcal{L}_\infty-$norm is defined as $\|f(\cdot)\|_\infty = \sup_{t\in\mathbb{R}} \|f(t)\|$. The time dependency of the variables is omitted when convenient.

II. Vehicle Modeling and Problem Definition

This section reviews the main features of the vehicle dynamics. Then, the related UI observer design problem is formulated. The vehicle parameters are given in Table I.

TABLE I
VEHICLE PARAMETERS.

Parameter	Symbol	Value
Distance from the CoG to front axle	l_f	1.3 [m]
Distance from the CoG to rear axle	l_r	1.6 [m]
Tire length contact	η_t	0.13 [m]
Steering gear ratio	R_s	16 [-]
Steering system damping	B_s	5.73 [-]
Manual steering column coefficient	K_p	0.5 [-]
Vehicle mass	M	2052 [kg]
Inertia of vehicle yaw moment	I_z	2800 [kgm^2]
Inertia of steering system	I_s	0.05 [kgm^2]
Front cornering stiffness	C_f	57000 [N/rad]
Rear cornering stiffness	C_r	59000 [N/rad]

A. Nonlinear Vehicle Dynamics

A nonlinear single track model is used to represent the vehicle motions in the horizontal plane, see Fig. 1. This model captures the essential vehicle dynamics, described as [35]

$$\begin{aligned} M\left(\dot{v}_x - r v_y\right) &= F_{xf}\cos\delta - F_{yf}\sin\delta + F_{xr} \\ M\left(\dot{v}_y + r v_x\right) &= F_{xf}\sin\delta + F_{yf}\cos\delta + F_{yr} \\ I_z\dot{r} &= l_f\left(F_{xf}\sin\delta + F_{yf}\cos\delta\right) - l_r F_{yr} \end{aligned} \tag{1}$$

where v_x is the longitudinal speed of the vehicle, v_y is the lateral speed, r is the yaw rate. The front/rear longitudinal and lateral tire forces F_{ki}, with $k \in \{x, y\}$ and $i \in \{f, r\}$, are caused by the contact between the tires and the road surface.

Several semi-empirical models are available in the literature to represent accurately the tire-road friction, such as Pacejka magic formula, LuGre model, etc. [5], which are not detailed here for brevity. The electronic power steering system can be modeled as [9]

$$\ddot{\delta}_d = \frac{T_{s\beta}}{I_s}\beta + \frac{T_{sr}}{I_s}r - \frac{T_{s\beta}}{R_s I_s}\delta_d - \frac{B_s}{I_s}\dot{\delta}_d + \frac{1}{I_s}T_s \qquad (2)$$

where δ_d is the driver's steering angle, β is the sideslip angle at the center of gravity (CoG) with

$$\beta = \arctan\left(\frac{v_y}{v_x}\right), \quad T_{s\beta} = \frac{2K_p C_f \eta_t}{R_s}, \quad T_{sr} = \frac{2K_p C_f \eta_t}{R_s}\frac{l_f}{v_x}.$$

The steering torque $T_s = T_a + T_d$ is composed of the *known* electrical assistance torque and the *unknown* driver torque.

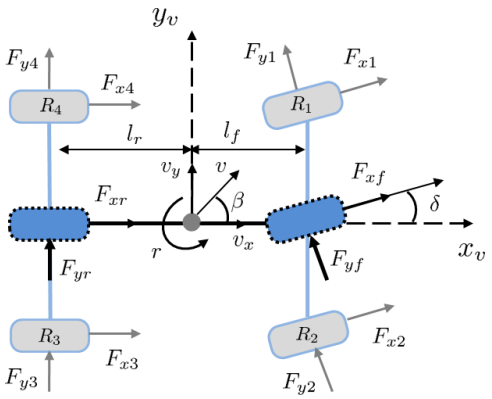

Fig. 1. Schematic of a two degrees-of-freedoms vehicle model.

B. Observer Problem Statement

As stated previously, despite its crucial importance to active safety control systems, the real-time information on the vehicle dynamics and the driver's torque cannot be always obtained from onboard sensors. Here, we provide a cost-effective solution to reconstruct such information though an unknown input observer which satisfies the following requirements.

- The new UI observer can be easily designed and implemented with only measurements from low-cost sensors.
- The estimation errors of both vehicle dynamics and driver's torque are norm-bounded which can be set *arbitrarily* small via an LMI-based optimization problem.
- The estimation performance and the robustness with respect to the time-varying vehicle speed can be guaranteed with Lyapunov stability arguments.

To meet these specifications, we propose in Section IV a new LPV unknown input observer design method.

III. LPV Representation of Vehicle System

We represent hereafter the vehicle system in a polytopic LPV form which is suitable for observer design purposes.

A. Observer-Based Vehicle System

To derive the observer-based vehicle model, we assume that [35]: (i) the vehicle speed is a time-varying parameter with a *limited* variation rate; (ii) the lateral tire forces are proportional to the slip angles of each axle; (iii) the small angle assumption is considered. Note that these assumptions are appropriate for normal driving under mild acceleration conditions. Then, the lateral tire forces can be modeled as follows:

$$F_{yf} = 2C_f\alpha_f, \quad F_{yr} = 2C_r\alpha_r \qquad (3)$$

where the sideslip angles of the front and rear tires are respectively given by

$$\alpha_f = \delta - \frac{v_y + l_f r}{v_x}, \quad \alpha_r = \frac{l_r r - v_y}{v_x}.$$

Remark that the relation between the driver's steering angle δ_d and the vehicle steering angle δ is given as $\delta_d = R_s\delta$. From (1) and (3), the vehicle lateral dynamics can be obtained in the following form:

$$\begin{bmatrix}\dot{\beta}\\ \dot{r}\end{bmatrix} = \begin{bmatrix}a_{11} & a_{12}\\ a_{21} & a_{22}\end{bmatrix}\begin{bmatrix}\beta\\ r\end{bmatrix} + \begin{bmatrix}b_1\\ b_2\end{bmatrix}\delta. \qquad (4)$$

The elements of the system matrices in (4) are given by

$$a_{11} = -\frac{2(C_r + C_f)}{Mv_x}, \quad a_{12} = \frac{2(l_rC_r - l_fC_f)}{Mv_x^2} - 1$$
$$a_{21} = \frac{2(l_rC_r - l_fC_f)}{I_z}, \quad a_{22} = \frac{-2(l_r^2C_r + l_f^2C_f)}{I_z v_x}$$
$$b_1 = \frac{2C_f}{Mv_x}, \quad b_2 = \frac{2l_fC_f}{I_z}.$$

From (2) and (4), we obtain the vehicle state-space model

$$\boldsymbol{\Sigma}_v(v_x): \quad \dot{\mathbf{x}} = A(v_x)\mathbf{x} + B\mathbf{u} + D\mathbf{d} \qquad (5)$$

where $\mathbf{x} = \begin{bmatrix}\beta & r & \delta & \dot{\delta}\end{bmatrix}^\top$ is the vehicle state, $\mathbf{u} = T_a$ is the known input, and $\mathbf{d} = T_d$ is the unknown input. The system matrices of (5) are given as follows:

$$A(v_x) = \begin{bmatrix}a_{11} & a_{12} & b_1 & 0\\ a_{21} & a_{22} & b_2 & 0\\ 0 & 0 & 0 & 1\\ a_{41} & a_{42} & a_{43} & a_{44}\end{bmatrix}, \quad B = D = \begin{bmatrix}0\\ 0\\ 0\\ \frac{1}{R_sI_s}\end{bmatrix}$$

where

$$a_{41} = \frac{T_{s\beta}}{R_sI_s}, \quad a_{42} = \frac{T_{sr}}{R_sI_s}, \quad a_{43} = -\frac{T_{s\beta}}{R_sI_s}, \quad a_{44} = -\frac{B_s}{I_s}.$$

For the vehicle system (5), the yaw rate r can be measured by an inertial navigation system. The steering angle δ and the steering rate $\dot{\delta}$ are obtained from an optical encoder. The sideslip angle β can be measured by a Correvit optical sensor. However, due to the excessive cost of Correvit sensors, the measurement of β is not available in practice. Therefore, the output equation of system (5) is given by

$$\mathbf{y} = C\mathbf{x}, \quad C = \begin{bmatrix}0 & 1 & 0 & 0\\ 0 & 0 & 1 & 0\\ 0 & 0 & 0 & 1\end{bmatrix}.$$

For observer design, we reformulate in the sequel the vehicle system $\boldsymbol{\Sigma}_v(v_x)$ in a numerically tractable LPV representation.

B. Polytopic LPV Representation of Vehicle System

Note that the vehicle dynamics in (5) depends on two speed-related terms $\frac{1}{v_x}$ and $\frac{1}{v_x^2}$, which are measured and bounded. For observer design, we consider the following bounds:

$$v_{\min} \leq v_x \leq v_{\max}, \quad v_{\min} = 5 \text{ [m/s]}, \ v_{\max} = 35 \text{ [m/s]}.$$

Let us define the parameter vector $\theta^*(t) = \begin{bmatrix} \frac{1}{v_x} & \frac{1}{v_x^2} \end{bmatrix}^\top$. These two parameters form a convex hull Θ^* with four vertices

$$\theta_{v1} = \begin{bmatrix} \frac{1}{v_{\min}} & \frac{1}{v_{\min}^2} \end{bmatrix}^\top, \qquad \theta_{v2} = \begin{bmatrix} \frac{1}{v_{\min}} & \frac{1}{v_{\max}^2} \end{bmatrix}^\top$$
$$\theta_{v3} = \begin{bmatrix} \frac{1}{v_{\max}} & \frac{1}{v_{\max}^2} \end{bmatrix}^\top, \qquad \theta_{v4} = \begin{bmatrix} \frac{1}{v_{\max}} & \frac{1}{v_{\min}^2} \end{bmatrix}^\top.$$

Such a parameter polytope Θ^* leads to design conservatism and numerical complexity since $\frac{1}{v_x}$ and $\frac{1}{v_x^2}$ are *separately* considered despite its strong dependency. To avoid this drawback and to reduce significantly the numerical complexity of the observer structure, we make use of the following variable change and the Taylor's approximation [9]:

$$\frac{1}{v_x} = \frac{1}{v_0} + \frac{1}{v_1}\theta, \quad \frac{1}{v_x^2} \simeq \frac{1}{v_0^2}\left(1 + 2\frac{v_0}{v_1}\theta\right) \tag{6}$$

where $v_0 = \frac{2v_{\min}v_{\max}}{v_{\min}+v_{\max}}$ and $v_1 = \frac{-2v_{\min}v_{\max}}{v_{\max}-v_{\min}}$. The time-varying parameter $\theta(t)$ in (6) verifies

$$\theta_{\min} \leq \theta \leq \theta_{\max}, \quad \theta_{\min} = -1, \quad \theta_{\max} = 1. \tag{7}$$

Since $v_x = v_{\min}$ for $\theta = \theta_{\min}$ and $v_x = v_{\max}$ for $\theta = \theta_{\max}$, the new parameter θ can be used to describe the variation of v_x between its lower and upper bounds.

Substituting (6) into (5), then the dynamics of the corresponding vehicle model

$$\boldsymbol{\Sigma}_v(\theta): \quad \begin{cases} \dot{\mathbf{x}} = A(\theta)\mathbf{x} + B\mathbf{u} + D\mathbf{d} \\ \mathbf{y} = C\mathbf{x} \end{cases}$$

depends *linearly* on θ. Using the sector nonlinearity approach [36, Chap. 2], the vehicle model $\boldsymbol{\Sigma}_v(\theta)$ can be *exactly* represented in the following polytopic LPV form:

$$\boldsymbol{\Sigma}_v(\theta): \quad \begin{cases} \dot{\mathbf{x}} = \sum_{i=1}^{2} \eta_i(\theta) A_i\mathbf{x} + B\mathbf{u} + D\mathbf{d} \\ \mathbf{y} = C\mathbf{x} \end{cases} \tag{8}$$

where the scalar membership functions are given by

$$\begin{aligned} \eta_1(\theta) &= \frac{1}{2}(1-\theta), \quad \eta_2(\theta) = 1 - \eta_1(\theta) \\ A_1 &= A(\theta_{\min}), \qquad A_2 = A(\theta_{\max}). \end{aligned} \tag{9}$$

Remark 1. Using the variable change together with the Taylor's approximation in (6), the number of vertices is reduced from four to two. From the practical viewpoint, the induced approximation error is expected to be small over the whole vehicle system (5) since only a part of the element a_{12} of matrix $A(v_x)$ is affected by this approximation. This is also justified by experimental results presented in Section V.

Remark 2. To limit the theoretical kinematic centripetal acceleration of the vehicle [37], the following bounds of vehicle acceleration are considered:

$$a_{\min} \leq a_x = \dot{v}_x \leq a_{\max}, \quad a_{\max} = -a_{\min} = 4 \text{ [m/s}^2\text{]}. \tag{10}$$

Then, it follows from (6) and (10) that

$$\frac{a_{\min}}{a_0} \leq \dot{\theta} \leq \frac{a_{\max}}{a_0}, \quad a_0 = -\frac{v_0^2}{v_1}. \tag{11}$$

As shown in Remark 3, exploiting simultaneously the bounds of both the vehicle speed (7) and the acceleration (11) in the observer design allows reducing further the conservatism.

IV. $\mathcal{L}_\infty$ Design of LPV Unknown Input Observers

To estimate simultaneously the vehicle dynamics and the driver torque, we present hereafter a set of LMIs to design UI observers. For generality, LPV systems in a general form are considered for theoretical development.

A. Problem Definition

Consider an LPV system with the state-space realization

$$\begin{aligned} \dot{\mathbf{x}} &= A(\theta)\mathbf{x} + B(\theta)\mathbf{u} + D(\theta)\mathbf{d} \\ \mathbf{y} &= C(\theta)\mathbf{x}, \quad \mathbf{x}(0) = \mathbf{x}_0 \end{aligned} \tag{12}$$

where $\mathbf{x} \in \mathbb{R}^{n_x}$ is the state, $\mathbf{u} \in \mathbb{R}^{n_u}$ is the known input, $\mathbf{d} \in \mathbb{R}^{n_d}$ is the unknown input, and $\mathbf{y}$ is the measured output. The scheduling variable $\theta \in \mathbb{R}^p$ and its rate of variation $\dot{\theta}$ are smooth and respectively valued in the hypercubes

$$\Theta = \{(\theta_1, \ldots, \theta_p)^\top : \ \theta_j \in [\underline{\theta}_j, \overline{\theta}_j], \ j \in \Omega_p\}$$
$$\Theta_d = \{(\dot{\theta}_1, \ldots, \dot{\theta}_p)^\top : \ \dot{\theta}_j \in [\underline{\upsilon}_j, \overline{\upsilon}_j], \ j \in \Omega_p\}$$

where $\underline{\theta}_j \leq \overline{\theta}_j$ (respectively $\underline{\upsilon}_j \leq \overline{\upsilon}_j$) are *known* lower and upper bounds on θ_j (respectively $\dot{\theta}_j$), for $j \in \Omega_p$. Assume that the time-varying state-space matrices $\Pi(\theta)$ of (12), with $\Pi \in \{A, B, C, D\}$, are continuous on the hypercube Θ. Then, using the sector nonlinearity approach in [36, Chap. 2], these state-space matrices can be *equivalently* represented by

$$\begin{aligned} A(\theta) &= \sum_{i=1}^{N} \eta_i(\theta) A_i, \quad B(\theta) = \sum_{i=1}^{N} \eta_i(\theta) B_i \\ C(\theta) &= \sum_{i=1}^{N} \eta_i(\theta) C_i, \quad D(\theta) = \sum_{i=1}^{N} \eta_i(\theta) D_i \end{aligned} \tag{13}$$

with $N = 2^p$ and $\Pi_i = \Pi(\theta)|_{\eta_i(\theta)=1}$, for $\forall \Pi \in \{A, B, C, D\}$. The membership functions $\eta_i(\theta)$, $i \in \Omega_N$, in (13) satisfy

$$\eta_i(\theta) \geq 0, \quad \sum_{i=1}^{N} \eta_i(\theta) = 1, \quad \sum_{i=1}^{N} \dot{\eta}_i(\theta) = 0, \quad \forall \theta \in \Theta.$$

Since $(\theta, \dot{\theta}) \in \Theta \times \Theta_d$, the lower bound ϕ_{i1} and the upper bound ϕ_{i2} of $\dot{\eta}_i(\theta)$ can be easily obtained as follows:

$$\dot{\eta}_i(\theta) \in \left[\phi_{i1}, \quad \phi_{i2}\right], \quad \phi_{i1} \leq \phi_{i2}, \quad i \in \Omega_N. \tag{14}$$

As an example, these bounds of the considered vehicle system can be derived from (7) and (11) as

$$\phi_{11} \leq \dot{\eta}_1(\theta) \leq \phi_{12}, \quad \phi_{21} \leq \dot{\eta}_2(\theta) \leq \phi_{22}$$

where

$$\phi_{11} = \frac{-a_{\max}}{2a_0}, \quad \phi_{12} = \frac{-a_{\min}}{2a_0}, \quad \phi_{21} = \frac{a_{\min}}{2a_0}, \quad \phi_{22} = \frac{a_{\max}}{2a_0}.$$

For the observer design, the following standard assumptions are considered for LPV system (12).

- The pair $(A(\theta), C(\theta))$ is detectable, for $\forall \theta \in \Theta$.
- The matrix $D(\theta)$ is of full-column rank, for $\forall \theta \in \Theta$.
- The unknown input $\mathbf{d}$ is bounded in amplitude.

Note that these assumptions are naturally verified for the vehicle model $\mathbf{\Sigma}_v(\theta)$ defined in (8).

We propose a Luenberger-type observer in the form

$$\begin{aligned} \dot{\hat{\mathbf{x}}} &= A(\theta)\hat{\mathbf{x}} + B(\theta)\mathbf{u} + D(\theta)\hat{\mathbf{d}} + \mathcal{M}(\theta)(\hat{\mathbf{y}} - \mathbf{y}) \\ \hat{\mathbf{y}} &= C(\theta)\hat{\mathbf{x}}, \quad \hat{\mathbf{x}}(0) = \hat{\mathbf{x}}_0 \end{aligned} \tag{15}$$

where $\hat{\mathbf{x}}(t)$ is the estimate of the state vector $\mathbf{x}(t)$, and $\hat{\mathbf{d}}(t)$ is the estimate of the unknown input $\mathbf{d}(t)$. The parameter-dependent observer gain $\mathcal{M}(\theta)$ is specified in Theorem 1. Let $\mathbf{e} = \hat{\mathbf{x}} - \mathbf{x}$ be the sate estimation error and $\mathbf{e}_d = \hat{\mathbf{d}} - \mathbf{d}$ be the estimation error of the UI. Then, the observer error dynamics is represented as

$$\dot{\mathbf{e}} = \hat{A}(\theta)\mathbf{e} + D(\theta)\mathbf{e}_d \tag{16}$$

with $\hat{A}(\theta) = A(\theta) + \mathcal{M}(\theta)C(\theta)$. The performance output associated with the state estimation error is defined as

$$\mathbf{z} = F(\theta)\mathbf{e} = \sum_{i=1}^{N} \eta_i(\theta) F_i \mathbf{e}. \tag{17}$$

We are now in the position to formulate the observer design problem related to the error dynamics (16).

Problem 1. Given an LPV system (12) with $(\theta, \dot{\theta}) \in \Theta \times \Theta_d$, $\forall t > 0$. Determine an observer gain $\mathcal{M}(\theta)$ such that the LPV observer (15) results in an input-to-state stable error dynamics with a guaranteed $\mathcal{L}_\infty-$gain performance. This means that the following closed-loop properties hold for system (16).

- If $\mathbf{e}_d(t) = 0$, for $\forall t \in \mathbb{R}_+$, the error dynamics (16) is globally exponentially stable.
- If $\mathbf{e}_d(t) \neq 0$, for $\forall t \in \mathbb{R}_+$, the state error is uniformly bounded for any initial condition $\mathbf{e}(0)$ and any bounded input $\mathbf{e}_d$. Moreover, the performance output (17) satisfies

$$\lim_{t \to \infty} \sup \|\mathbf{z}\| \leq \gamma \|\mathbf{e}_d\|_\infty, \quad \gamma > 0 \tag{18}$$

  where the $\mathcal{L}_\infty-$gain γ is specified in Theorem 1.

From (17) and (18), we remark that a smaller value of the $\mathcal{L}_\infty-$gain γ leads to a better estimation performance.

B. LMI-Based Optimization for LPV Observer Design

The following theorem provides LMI conditions to design an UI observer (15) for LPV systems of the form (12).

Theorem 1. Given an LPV system (12) with $(\theta, \dot{\theta}) \in \Theta \times \Theta_d$, and a positive scalar α. Assume there exist symmetric matrices $X \in \mathbb{R}^{n_x \times n_x}$, $P_i \in \mathbb{R}^{n_x \times n_x}$, matrices $L_i \in \mathbb{R}^{n_x \times n_y}$, for $i \in \Omega_N$, and positive scalars μ, ν such that the following optimization problem is feasible:

$$\underset{\xi_i,\ i \in \Omega_N}{\texttt{minimize}} \quad \mu + \nu$$

subject to

$$P_i + X \succ 0 \tag{19}$$

$$\begin{bmatrix} P_i + X & \star \\ F_i & \mu I \end{bmatrix} \succeq 0 \tag{20}$$

$$\Upsilon_{ii}^{kl} \preceq 0, \quad \Upsilon_{ij}^{kl} + \Upsilon_{ji}^{kl} \preceq 0 \tag{21}$$

where $\xi_i = (\mu, \nu, X, P_i, L_i)$ and $i, j \in \Omega_N$, $i < j$, $k \in \Omega_{N-1}$, $l \in \Omega_2$. The quantity Υ_{ij}^{kl} in (21) is defined as follows:

$$\Upsilon_{ij}^{kl} = \mathrm{He}\begin{bmatrix} P_i A_j + L_i C_j + \alpha P_i + \frac{1}{2}\Psi & (P_i + X)D_j \\ 0 & -\alpha\nu I \end{bmatrix} \tag{22}$$

$$\Psi = \phi_{kl}(P_k + X - P_N) + \phi_{Nl} X + 2XA_j + 2\alpha X.$$

Then, the LPV observer (15) with the parameter-dependent gain defined as $\mathcal{M}(\theta) = \mathcal{P}(\theta)^{-1} L(\theta)$ and

$$\mathcal{P}(\theta) = \sum_{i=1}^{N} \eta_i(\theta)(P_i + X), \quad L(\theta) = \sum_{i=1}^{N} \eta_i(\theta) L_i \tag{23}$$

ensures that the error dynamics (16) together with its associated performance output (17) verify the closed-loop properties given in Problem 1. Moreover, the guaranteed $\mathcal{L}_\infty-$gain performance is defined as $\gamma = \sqrt{\nu\mu}$.

Proof. For stability analysis and observer design, we consider the following parameter-dependent Lyapunov function:

$$\mathcal{V}(\mathbf{e}) = \mathbf{e}^\top \mathcal{P}(\theta)\mathbf{e}. \tag{24}$$

Condition (19) guarantees that $\mathcal{P}(\theta)$ is positive definite for $\forall \theta \in \Theta$. Hence, $\mathcal{V}(\mathbf{e})$ is a proper Lyapunov function candidate.

Since $\sum_{i=1}^{N} \dot{\eta}_i(\theta) = 0$, for any matrix X, it follows that

$$\begin{aligned} \dot{\mathcal{P}}(\theta) &= \sum_{k=1}^{N-1} \dot{\eta}_k(\theta)(P_k + X) + \dot{\eta}_N(\theta)(P_N + X) \\ &= \sum_{k=1}^{N-1} \dot{\eta}_k(\theta)(P_k + X - P_N) + \dot{\eta}_N(\theta) X. \end{aligned} \tag{25}$$

For any $\phi_{k1} \leq \dot{\eta}_k(\theta) \leq \phi_{k2}$ in (14), it follows that

$$\dot{\eta}_k(\theta) = \omega_{k1}(\theta)\phi_{k1} + \omega_{k2}(\theta)\phi_{k2}, \quad k \in \Omega_N \tag{26}$$

where

$$\omega_{k1}(\theta) = \frac{\phi_{k2} - \dot{\eta}_k(\theta)}{\phi_{k2} - \phi_{k1}}, \quad \omega_{k2}(\theta) = \frac{\dot{\eta}_k(\theta) - \phi_{k1}}{\phi_{k2} - \phi_{k1}}. \tag{27}$$

Note also that $\omega_{kl}(\theta) \geq 0$, $\sum_{l=1}^{2} \omega_{kl}(\theta) = 1$, for $\forall k \in \Omega_N$. From (25), (26) and (27), $\dot{\mathcal{P}}(\theta)$ can be *exactly* represented as

$$\dot{\mathcal{P}}(\theta) = \sum_{k=1}^{N-1} \sum_{l=1}^{2} [\omega_{kl}(\theta)\phi_{kl}\mathcal{X} + \omega_{Nl}(\theta)\phi_{Nl} X] \tag{28}$$

with $\mathcal{X} = P_k + X - P_N$. Using expressions (28) and (22), (21) implies that

$$\Gamma_{ii}(\theta) \preceq 0, \quad \Gamma_{ij}(\theta) + \Gamma_{ji}(\theta) \preceq 0, \ i, j \in \Omega_N, \ i < j \tag{29}$$

where

$$\Gamma_{ij}(\theta) = \mathrm{He}\begin{bmatrix} P_iA_j + L_iC_j + \alpha P_i + \frac{1}{2}\Lambda(\theta) & (P_i+X)D_j \\ 0 & -\alpha\nu I \end{bmatrix}$$
$$\Lambda(\theta) = \dot{\mathcal{P}}(\theta) + 2XA_j + 2\alpha X.$$

Since $\eta_i(\theta) \geq 0$, $\forall i \in \Omega_N$, it follows from (29) that

$$\sum_{i=1}^{N}\eta_i(\theta)^2\Gamma_{ii}(\theta) + \sum_{i=1}^{N}\sum_{i<j}^{N}\eta_i(\theta)\eta_j(\theta)\left(\Gamma_{ij}(\theta)+\Gamma_{ji}(\theta)\right) = \sum_{i=1}^{N}\sum_{j=1}^{N}\eta_i(\theta)\eta_j(\theta)\Gamma_{ij}(\theta) \preceq 0. \quad (30)$$

Inequality (30) can be rewritten in the following form:

$$\mathrm{He}\begin{bmatrix} \mathcal{W}(\theta) + \alpha\mathcal{P}(\theta) + \frac{1}{2}\dot{\mathcal{P}}(\theta) & \mathcal{P}(\theta)D(\theta) \\ 0 & -\alpha\nu I \end{bmatrix} \preceq 0 \quad (31)$$

where $\mathcal{W}(\theta) = \mathcal{P}(\theta)A(\theta) + L(\theta)C(\theta)$. Pre- and postmultiplying (31) with $\begin{bmatrix}\mathbf{e}^\top & \mathbf{e}_d^\top\end{bmatrix}$ and its transpose leads to the following condition after some algebraic manipulations:

$$\dot{\mathcal{V}}(\mathbf{e}) \leq -2\alpha\left(\mathcal{V}(\mathbf{e}) - \nu\|\mathbf{e}_d\|^2\right) \quad (32)$$

where $\dot{\mathcal{V}}(\mathbf{e})$ is the time-derivative of the Lyapunov function defined in (24) along the solution of the error dynamics (16). It is clear that (32) implies the following inequality:

$$\dot{\mathcal{V}}(\mathbf{e}) \leq -2\alpha\left(\mathcal{V}(\mathbf{e}) - \nu\|\mathbf{e}_d\|_\infty^2\right). \quad (33)$$

Multiplying both sides of (33) by $e^{2\alpha t}$, then integrating over $[t_0, t]$, we obtain

$$e^{2\alpha t}\mathcal{V}(\mathbf{e}) \leq e^{2\alpha t_0}\mathcal{V}(\mathbf{e}_0) + 2\alpha\nu\|\mathbf{e}_d\|_\infty^2\int_{t_0}^{t}e^{2\alpha\tau}d\tau = e^{2\alpha t_0}\mathcal{V}(\mathbf{e}_0) + \nu\|\mathbf{e}_d\|_\infty^2\left(e^{2\alpha t} - e^{2\alpha t_0}\right) \quad (34)$$

with $\mathbf{e}_0 = \hat{\mathbf{x}}_0 - \mathbf{x}_0$. It follows from (34) that

$$\mathcal{V}(\mathbf{e}) \leq e^{-2\alpha(t-t_0)}\mathcal{V}(\mathbf{e}_0) + \nu\|\mathbf{e}_d\|_\infty^2\left(1 - e^{-2\alpha(t-t_0)}\right) \leq e^{-2\alpha(t-t_0)}\mathcal{V}(\mathbf{e}_0) + \nu\|\mathbf{e}_d\|_\infty^2. \quad (35)$$

Considering the Lyapunov function (24), one has

$$\alpha_1\|\mathbf{e}\|^2 \leq \mathcal{V}(\mathbf{e}) \leq \alpha_2\|\mathbf{e}\|^2 \quad (36)$$

with $\alpha_1 = \min_{i\in\Omega_N}\lambda_{\min}(P_i + X)$ and $\alpha_2 = \max_{i\in\Omega_N}\lambda_{\max}(P_i + X)$. It follows from (35) and (36) that

$$\alpha_1\|\mathbf{e}\|^2 \leq \alpha_2 e^{-2\alpha(t-t_0)}\|\mathbf{e}_0\|^2 + \nu\|\mathbf{e}_d\|_\infty^2$$

which, in turn, implies that

$$\|\mathbf{e}\| \leq \sqrt{\frac{\alpha_2}{\alpha_1}}e^{-\alpha(t-t_0)}\|\mathbf{e}_0\| + \sqrt{\frac{\nu}{\alpha_1}}\|\mathbf{e}_d\|_\infty. \quad (37)$$

Inequality (37) guarantees that the observer error dynamics is globally bounded for any initial condition $\mathbf{e}_0$ and any bounded unknown input $\mathbf{d}$. Moreover, if $\mathbf{e}_d(t) = 0$, $\forall t \in \mathbb{R}_+$, then the error dynamics is *exponentially* stable about the origin.

Multiplying (20) by $\eta_i(\theta) \geq 0$ and summing up for all $i \in \Omega_N$, we obtain

$$\begin{bmatrix}\mathcal{P}(\theta) & \star \\ F(\theta) & \mu I\end{bmatrix} \succeq 0. \quad (38)$$

By the well-known Schur complement lemma [34], condition (38) is shown to be equivalent to

$$\mathcal{P}(\theta) - \mu^{-1}F(\theta)^\top F(\theta) \succeq 0. \quad (39)$$

Pre- and postmultiplying (39) with $\mathbf{e}^\top$ and its transpose while considering the performance output (17), we obtain

$$\|\mathbf{z}\|^2 \leq \mu\mathcal{V}(\mathbf{e}). \quad (40)$$

It follows from (35) and (40) that

$$\|\mathbf{z}\| \leq \sqrt{\mu\mathcal{V}(\mathbf{e}_0)}e^{-\alpha(t-t_0)} + \sqrt{\nu\mu}\|\mathbf{e}_d\|_\infty. \quad (41)$$

For any initial condition $\mathbf{e}_0$ and any bounded signal $\mathbf{e}_d$, it follows from (41) that

$$\lim_{t\to\infty}\sup\|\mathbf{z}\| \leq \gamma\|\mathbf{e}_d\|_\infty \quad (42)$$

with $\gamma = \sqrt{\nu\mu}$. Hence, all the closed-loop properties described in Problem 1 are now proved. This concludes the proof. □

Remark 3. To reduce the design conservatism, we introduce a slack variable X into the construction of the Lyapunov function (24). A similar idea has been presented in [38] for the stability analysis of Takagi-Sugeno fuzzy systems using fuzzy Lyapunov functions. However, here the Lyapunov matrices P_i, for $\forall i \in \Omega_N$, are not required to be definite positive as in most of LPV and/or fuzzy-model-based control and observation results in the literature [38], [39]. Moreover, *explicit* information on θ and $\dot{\theta}$, represented by the bounds ϕ_{kl}, for $k \in \Omega_N$, $l \in \Omega_2$, is exploited via using the parameter-dependent Lyapunov function (24) to reduce further the conservatism of the results. Indeed, if we impose $X = 0$, $P_1 = \cdots = P_N = P$, then the quadratic Lyapunov function $V(\mathbf{e}) = \mathbf{e}^\top P\mathbf{e}$ is recovered from (24). In addition, if (21) is feasible for *arbitrarily* large values of $|\phi_{kl}|$, then the only possible solution is such that $P_1 \approx \cdots \approx P_N$ and $X \approx 0$ to minimize the effect of $\phi_{kl}(P_k + X - P_N) + \phi_{Nl}X$ involved in (22). Hence, the proposed results include those derived from quadratic or poly-quadratic Lyapunov functions $\mathbf{V}(\mathbf{e}) = \mathbf{e}^\top\sum_{i=1}^{N}\eta_i(\theta)P_i\mathbf{e}$. Similar arguments on the conservatism relaxation using parameter-dependent Lyapunov functions can be found in [39].

Remark 4. Consider the error dynamics (16) with $\mathbf{z} = \mathbf{e}$. By minimizing γ, it follows directly from (42) that the estimation error $\mathbf{e}$ can be minimized. Moreover, if the optimization problem in Theorem 1 is feasible with *arbitrarily* small values of ν and μ, then the estimation error can be arbitrarily small.

C. Unknown Input Reconstruction with Norm-Bounded Error

From the design of LPV observer (15) in Theorem 1, we present hereafter a method to estimate the unknown input $\mathbf{d}(t)$. This method is similar to the equivalent-input-disturbance concept discussed in [40], [41].

For a given signal $z(t)$, let us denote its Laplace transform as $\mathfrak{Z}(s) = \mathcal{L}[z(t)]$. Then, the estimate $\hat{\mathbf{d}}(t)$ of the UI can be constructed in the Laplace domain as follows:

$$\hat{\mathfrak{D}}(s) = \mathbf{F}(s)\tilde{\mathfrak{D}}(s) \quad (43)$$

where $\tilde{\mathbf{d}}(t)$ is the modified UI estimate error, defined as

$$\tilde{\mathbf{d}}(t) = D(\theta)^{\dagger}\mathcal{M}(\theta)(\hat{\mathbf{y}}(t) - \mathbf{y}(t)) + \hat{\mathbf{d}}(t). \tag{44}$$

Note that $D(\theta)$ is full column rank, then

$$D(\theta)^{\dagger} = \left(D(\theta)^{\top}D(\theta)\right)^{-1}D(\theta)^{\top}$$

and $D(\theta)^{\dagger}D(\theta) = I$. In general, the low-pass filter $\mathbf{F}(s)$ in (43) can be of any form [40]. However, here we take $\mathbf{F}(s)$ in the following form for simplicity:

$$\mathbf{F}(s) = \frac{1}{T_f s + 1}. \tag{45}$$

The parameter T_f regulates the angular-frequency band for disturbance rejection which can be chosen as follows [40]:

$$T_f \leq \frac{1}{5 \sim 10}\frac{1}{\omega} \tag{46}$$

where ω is the highest angular frequency selected for disturbance rejection. From (43), (44) and (45), it follows that

$$\dot{\hat{\mathbf{d}}} = \frac{1}{T_f}D(\theta)^{\dagger}\mathcal{M}(\theta)(\hat{\mathbf{y}} - \mathbf{y}) = \frac{1}{T_f}D(\theta)^{\dagger}\mathcal{M}(\theta)C(\theta)\mathbf{e}. \tag{47}$$

Observe that the dynamics of the UI estimate $\hat{\mathbf{d}}$ is governed by the state estimation error. Recalling the observer error dynamics (16), multiplying both sides by $D(\theta)^{\dagger}$, we obtain

$$\mathbf{e}_d = D(\theta)^{\dagger}\left(\dot{\mathbf{e}} - \hat{A}(\theta)\mathbf{e}\right). \tag{48}$$

It follows from (48) that

$$\|\mathbf{e}_d\| \leq \|D(\theta)^{\dagger}\|\|\dot{\mathbf{e}}\| + \|D(\theta)^{\dagger}\hat{A}(\theta)\|\|\mathbf{e}\|.$$

Note that $\mathbf{e}_d$ is bounded with respect to the 2-norm of the state error $\mathbf{e}$ and its rate of variation $\dot{\mathbf{e}}$. By minimizing the $\mathcal{L}_{\infty}-$gain γ, it is expected to achieve an accurate reconstruction of the unknown input, see also Remark 4.

Remark 5. The proposed UI observer design method has many major practical and theoretical advantages compared to the available literature. First, remark in (47) that the time-derivatives of the system output and/or the time-varying parameters are not required for the UI reconstruction as in the recent work [24]. Second, the measured output is not required to be of the form $\mathbf{y} = C(\theta)\mathbf{x} + G(\theta)\mathbf{d}$, with a full row rank matrix $G(\theta)$, as most of UI decoupling approaches [32]. Third, we can avoid the assumption on the $k-$order time-derivative of the unknown input, *i.e.*, $\mathbf{d}^{(k)} \simeq 0$, required for the design of PMI observers [30], [33]. Note that to improve the estimation performance, the value of k may be significantly large which induces complexities/difficulties for real-time purposes. Moreover, compared to the UI observer in [11] with eight linear submodels and nonlinear membership functions to be computed online, our observer has a simple structure for real-time implementation with only two linear submodels and membership functions given in (9).

Remark 6. The new UI observer design is easily performed through LMI-based conditions in Theorem 1. Here, all numerical optimizations are solved with YALMIP toolbox [42].

V. Experimental Results and Comparative Studies

To demonstrate the effectiveness of the proposed $\mathcal{L}_{\infty}$ unknown input observer, this section presents experimental results carried out with the SHERPA driving simulator under various test scenarios. This interactive simulator is based on a Peugeot 206 mock-up fixed on a 6-axis Bosch Rexroth motion system, the overall is positioned in front of five flat panel displays providing a visual field of 240°, see Fig. 2. The simulator is equipped with a force feedback gas pedal to manage the vehicle speed. The SensoDrive force feedback steering wheel provides precisely the torque from the driver's hands. Moreover, the SHERPA simulator is fully instrumented to measure the vehicle dynamics. Using the SCANeR^{TM} Studio 1.6 environment, the proposed UI observer is implemented in the SHERPA simulator through Matlab/Simulink software.

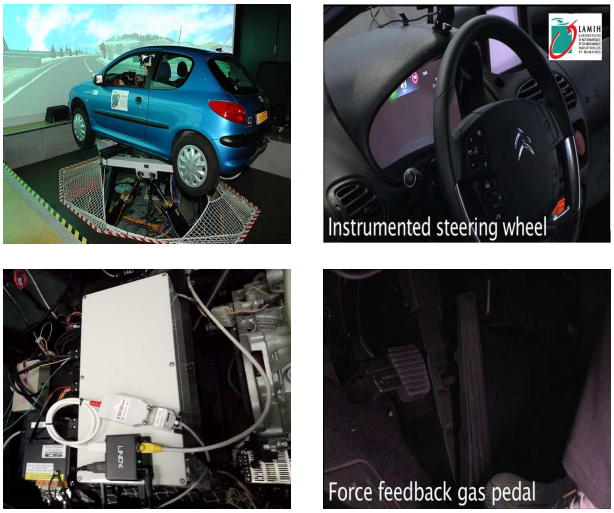

Fig. 2. SHERPA driving simulator (upper left). Steering system (upper right). Data acquisition system (bottom left). Active gas pedal (bottom right).

The decay rate α is related to the time performance of the error dynamics (16). A large value of this tuning parameter leads to a fast convergence time. However, the corresponding observer may induce some aggressive behaviors. Here, we select $\alpha = 5$ to guarantee a satisfactory error convergence. Note that a normal human driver produces torque input at 3 to 5 Hz on the steering wheel [7]. The value of T_f is chosen following (46) such that the filter bandwidth of $\mathbf{F}(s)$ covers the spectrum of the driver torque signal. As a result, the UI estimation frequency is much faster than the human input frequency, allowing to capture and estimate accurately any changes in the driver torque.

Taking $\mathbf{z} = \mathbf{e}$, the observer gains in (23) can be obtained from the LMI-based optimization in Theorem 1 as follows:

$$P_1 = \begin{bmatrix} 17039 & -14040 & 20624 & -60.373 \\ -14040 & 24802 & -45281 & 7.1634 \\ 20624 & -45281 & 63790 & 3.5945 \\ -60.373 & 7.1634 & 3.5945 & 131.5 \end{bmatrix}$$

$$P_2 = \begin{bmatrix} 11766 & -9277.9 & 18468 & -58.749 \\ -9277.9 & 14755 & -29701 & 9.3613 \\ 18468 & -29701 & 64869 & 1.9655 \\ -58.749 & 9.3613 & 1.9655 & 131.7 \end{bmatrix}$$

$$X = \begin{bmatrix} -2243.1 & 2623 & 509.74 & 1.3714 \\ 2623 & -4873.1 & 8767.8 & 1.4501 \\ 509.74 & 8767.8 & 6948.5 & 1.4405 \\ 1.3714 & 1.4501 & 1.4405 & 0.10012 \end{bmatrix}$$

$$L_1 = \begin{bmatrix} -31167 & 71163 & -944.47 \\ -81309 & -15362 & 77.736 \\ -24591 & -57230 & 147.86 \\ 390.4 & -665.63 & -99930 \end{bmatrix}$$

$$L_2 = \begin{bmatrix} 4376.3 & 96980 & -2028.6 \\ -98987 & 1000.5 & 6.0984 \\ 13408 & -24273 & 537.35 \\ -22.816 & -2098.2 & -99978 \end{bmatrix}.$$

The corresponding $\mathcal{L}_\infty-$gain is given by $\gamma = 0.002$. Note that P_1 is not positive definite. Solving the optimization in Theorem 1 under the same setting with $P_1 = P_2 = P$ and $X = 0$, *i.e.*, quadratic approach, we obtain $\gamma_{quad} = 0.007 > \gamma$. This numerically illustrates the statements in Remark 3. Since γ is very small, an accurate estimation of both vehicle dynamics and unknown driver torque can be achieved as shown in the following driving test scenarios.

A. Scenario 1: Manual Driving in Real-World Conditions

For this scenario, we consider a normal *manual* driving condition without assistive torque, *i.e.*, $T_a = 0$. To this end, the human driver manually performs the path following task on the Satory test track, situated at 20 km west from Paris, France, see Fig. 3(a). The corresponding vehicle speed is managed by the driver and depicted in Fig. 3(b). Observe that this test track includes several tight bends which implies a high variation in the driver torque along the track. As indicated in Fig. 3, the proposed observer provides an excellent estimation performance with respect to both driver torque and lateral vehicle dynamics for normal driving situations. This is also numerically confirmed by the small error indices summarized in Table II. Note that E_{mean} is the average error, $E_{\max}$ is the maximal error, Std is the standard deviation of the estimation error, and RMS is the root-mean-square error. Note also that the unit [deg] is used here in place of [rad] to improve the readability of the numerical error results.

B. Scenario 2: Human Take-Over Driving Control

This scenario represents a driving situation where the human driver must *punctually* take over the vehicle control from a lane-keeping assist system at a constant speed $v_x = 14$ [m/s]. During this maneuver, the driver-automation conflict issue arises [26], which is also indicated by the opposite sign of the driver and assistive torques in Fig. 4(a). We can see in Fig. 4 that both the driver torque and the vehicle state are accurately estimated despite the presence of the opposite assistive torque. The statistics data on the estimation errors given in Table III numerically confirm the good estimation performance in this shared control driving situation.

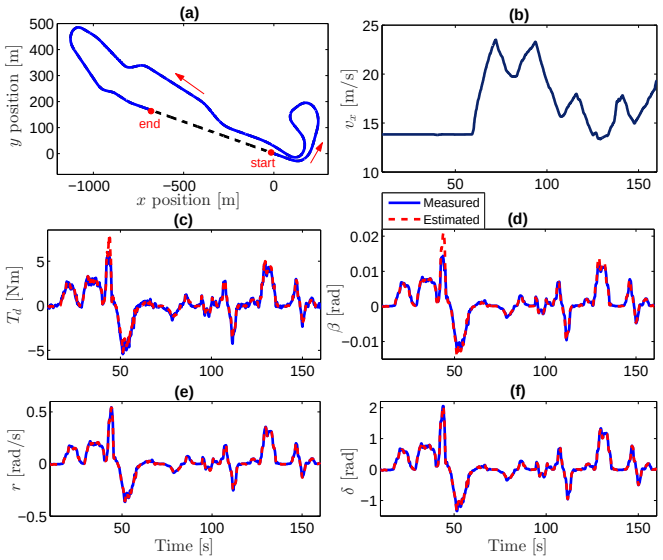

Fig. 3. Estimation performance obtained with real-world driving conditions. (a) Satory test track. (b) Vehicle speed profile. (c) Driver steering torque. (d) Sideslip angle. (e) Yaw rate. (f) Steering angle.

TABLE II
NUMERICAL STATISTICS ON ESTIMATION ERRORS FOR SCENARIO 1.

Error index	E_{mean}	$E_{\max}$	Std	RMS
T_d [Nm]	0.1595	2.6161	0.2442	0.2471
β [deg]	0.0194	0.5889	0.0527	0.0527
r [deg/s]	0.0155	0.2350	0.0211	0.0232
δ [deg]	0.1762	1.8720	0.2739	0.2746
$\dot{\delta}$ [deg/s]	0.0224	0.4007	0.0447	0.0448

TABLE III
NUMERICAL STATISTICS ON ESTIMATION ERRORS FOR SCENARIO 2.

Error index	E_{mean}	$E_{\max}$	Std	RMS
T_d [Nm]	0.3253	7.8076	0.6560	0.6608
β [deg]	0.0356	0.5911	0.0716	0.0716
r [deg/s]	0.0390	0.4630	0.0576	0.0589
δ [deg]	0.3011	8.1573	0.6891	0.6894
$\dot{\delta}$ [deg/s]	0.1855	15.7404	0.7107	0.7104

C. Scenario 3: Driving in an Extreme Situation

Aiming to test the limitations of the proposed LPV observer, this scenario does not represent a standard driving behavior. Here, the human driver performs a *zigzag* driving pattern on the road without any assistance, *i.e.*, $T_a = 0$. The time-varying speed profile corresponding to this test is shown in Fig. 5(a). As a result, the driver virtually creates a progressive lateral acceleration a_{lat} as depicted in Fig. 5(b). To examine in detail

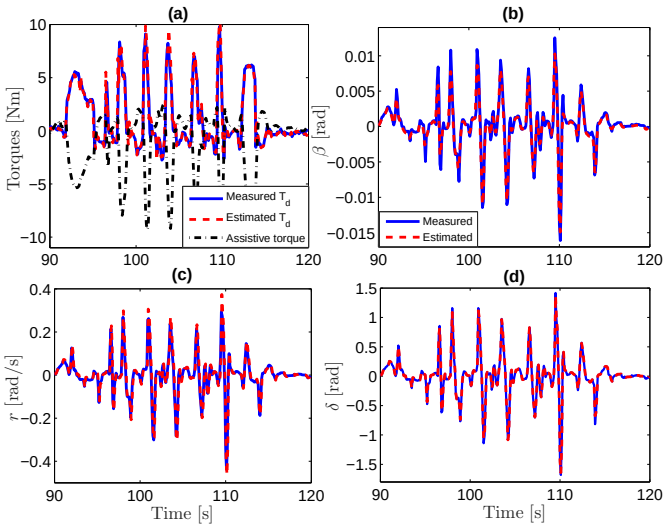

Fig. 4. Estimation performance in case of human take-over control. (a) Measured driver torque (solid line), estimated driver torque (dashed line), assistance steering torque (dash-dot line). (b) Sideslip angle. (c) Yaw rate. (d) Steering angle.

this scenario, two zooms are performed which correspond to two operating zones of the vehicle. For the first zoom corresponding to an operating zone with relatively small lateral acceleration, *i.e.*, $a_{lat} < 4$ [m/s^2]. Observe in Figs. 5(e), (f) that both the driver torque and the sideslip angle are accurately reconstructed within this zone. However, we note that the estimations are much less precise in the operating zone with $a_{lat} > 4$ [m/s^2]. This performance limitation is expected since the bicycle model used for the observer design in this work is rather valid for normal driving conditions with a reasonable level of lateral acceleration a_{lat}. Nevertheless, the estimation performance is globally satisfactory for this scenario test.

D. Scenario 4: Comparative Study with a PMI Observer

For this test, the vehicle is on a straight road section at a constant speed $v_x = 15$ [m/s]. The driver is also required to perform a zigzag driving pattern. Differently from Scenario 3, the driver now *jointly* controls the vehicle with the driving assistance system whose assistive torque T_a is presented in Fig. 6(a). The study goal here is twofold. First, a satisfactory estimation performance is experimentally verified with our LPV observer given by (15) and (47) in the case of sharp variations in the driver torque as indicated in Fig. 6. Second and more importantly, a comparison is performed with a PMI observer largely adopted in automotive applications [28], [29]. The $\mathcal{D}-$stability concept is incorporated in the observer design to improve the estimation performance as discussed in detail in [29]. Observe in Fig. 6 that both LPV observers provide almost similar performance for both the lateral dynamics and the unknown input T_d. In the case of high lateral accelerations, the proposed solution offers a better estimation in the sideslip angle and the driver torque as shown in Fig. 7. The numerical comparison results given in Table IV confirm these remarks. Note also that the particular interest of the new observer consists in its simplicity for online purposes since it is assumed

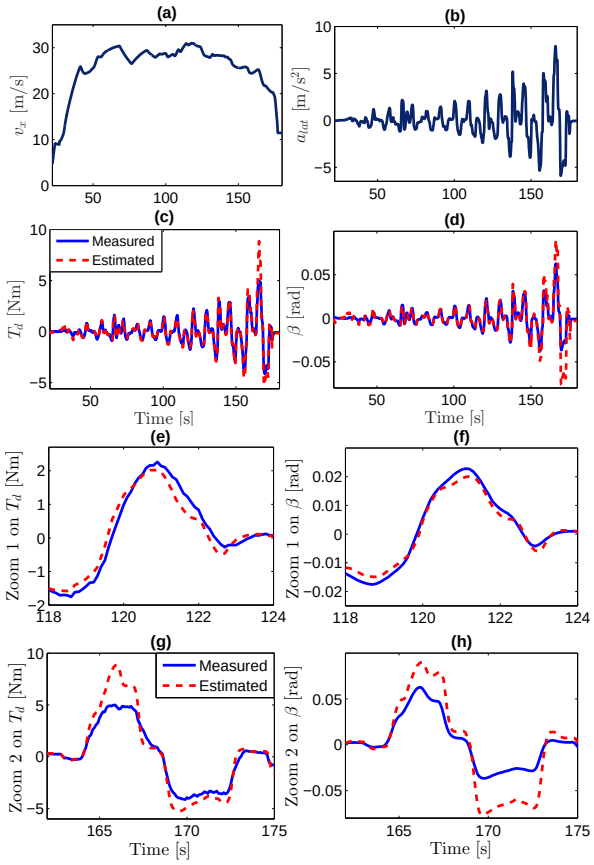

Fig. 5. Estimation performance obtained with an extreme driving situation. (a) Vehicle speed profile. (b) Vehicle lateral acceleration. (c) Driver steering torque. (d) Sideslip angle. (e) A zoom on driver torque at low lateral acceleration ($a_{lat} < 4$ [m/s^2]). (f) A zoom on sideslip angle at low lateral acceleration. (g) A zoom on driver torque at high lateral acceleration ($a_{lat} > 4$ [m/s^2]). (h) A zoom on sideslip angle at high lateral acceleration.

that $\ddot{T}_d = 0$ for the design of the PMI observer, which consequently has two more dimensions compared to ours, see Remark 5. Moreover, although both observers used for comparison are in polytopic form, the new LPV observer (15) only requires two linear submodels in place of four as the one in [29].

TABLE IV
COMPARISON ON THE ESTIMATION PERFORMANCE BETWEEN TWO OBSERVER DESIGNS.

Error index	Proposed observer	PMI observer [29]
E_{mean} T_d [Nm]	0.1956	0.2787
E_{mean} β [deg]	0.0100	0.0171
E_{max} T_d [Nm]	1.2069	2.3970
E_{max} β [deg]	0.0969	0.1112
Std T_d [Nm]	0.3570	0.4845
Std β [deg]	0.0176	0.0291
RMS T_d [Nm]	0.3640	0.4846
RMS β [deg]	0.0176	0.0291

VI. CONCLUDING REMARKS

This paper provides an effective LMI-based solution to estimate simultaneously the vehicle dynamics and the driver

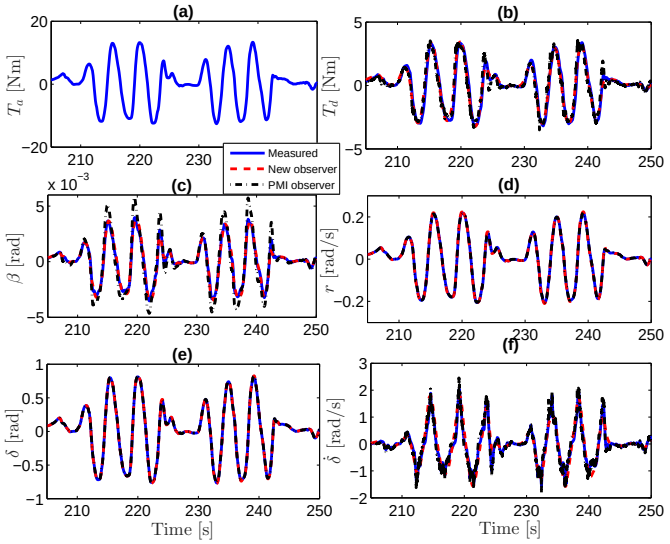

Fig. 6. Estimation performance comparison between the proposed solution and the PMI observer in [29]. (a) Assistance steering torque. (b) Driver torque. (c) Sideslip angle. (d) Yaw rate. (e) Steering angle. (f) Steering rate.

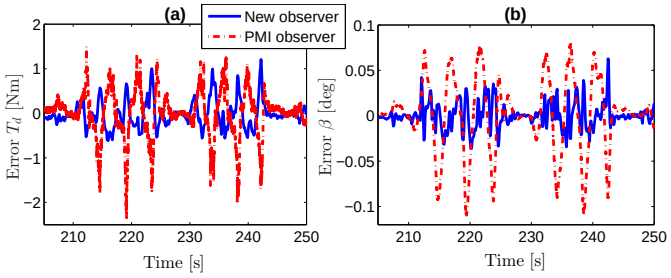

Fig. 7. Estimation errors obtained with the proposed solution and the PMI observer in [29]. (a) Driver torque error. (b) Sideslip angle error.

torque. To this end, the vehicle system is transformed into a polytopic LPV model with a reduced complexity to deal with time-varying vehicle speed while keeping a simple observer characterization. In particular, theoretical design is based on the use of a parameter-dependent Lyapunov function to exploit the information on the vehicle speed and acceleration bounds for conservatism reduction. The proposed unknown input observer can lead to arbitrarily small estimation errors by minimizing the guaranteed $\mathcal{L}_\infty-$gain performance. The effectiveness of the new observer design is experimentally verified with the real-time data of the SHERPA dynamic driving simulator. The interest of our method is also highlighted through a comparative study with respect to existing literature. For future works, taking into account of the nonlinearity and/or the uncertainty of the lateral tire forces should be investigated.

REFERENCES

[1] L. Li, D. Wen, N.-N. Zheng, and L.-C. Shen, "Cognitive cars: A new frontier for ADAS research," *IEEE Trans. Intell. Transp. Syst.*, vol. 13, no. 1, pp. 395–407, Mar. 2012.

[2] K. Bengler, K. Dietmayer, B. Farber, M. Maurer, C. Stiller, and H. Winner, "Three decades of driver assistance systems: Review and future perspectives," *IEEE Intell. Transp. Syst. Mag.*, vol. 6, no. 4, pp. 6–22, winter 2014.

[3] M. D. Lio, F. Biral, E. Bertolazzi, M. Galvani, P. Bosetti, D. Windridge, A. Saroldi, and F. Tango, "Artificial co-drivers as a universal enabling technology for future intelligent vehicles and transportation systems," *IEEE Trans. Intell. Transp. Syst.*, vol. 16, no. 1, pp. 244–263, Feb. 2015.

[4] H. Guo, Z. Yin, D. Cao, H. Chen, and C. Lv, "A review of estimation for vehicle tire-road interactions toward automated driving," *IEEE Trans. Syst., Man, Cybern.: Syst.*, vol. 49, no. 1, pp. 14–30, Jan. 2019.

[5] L. Li, F.-Y. Wang, and Q. Zhou, "Integrated longitudinal and lateral tire/road friction modeling and monitoring for vehicle motion control," *IEEE Trans. Intell. Transp. Syst.*, vol. 7, no. 1, pp. 1–19, Mar. 2006.

[6] E. Hashemi, M. Pirani, A. Khajepour, B. Fidan, A. Kasaiezadeh, and S. Chen, "Opinion dynamics-based vehicle velocity estimation and diagnosis," *IEEE Trans. Intell. Transp. Syst.*, vol. 19, no. 7, pp. 2142–2148, July 2018.

[7] X. Wang, L. Guo, and Y. Jia, "Online sensing of human steering intervention torque for autonomous driving actuation systems," *IEEE Sens. J.*, vol. 18, no. 8, pp. 3444–3453, Apr. 2018.

[8] H. Zhang, X. Huang, J. Wang, and H. R. Karimi, "Robust energy-to-peak sideslip angle estimation with applications to ground vehicles," *Mechatronics*, vol. 30, pp. 338–347, Sept. 2015.

[9] A.-T. Nguyen, C. Sentouh, and J.-C. Popieul, "Sensor reduction for driver-automation shared steering control via an adaptive authority allocation strategy," *IEEE/ASME Trans. Mechatron.*, vol. 23, no. 1, pp. 5–16, Feb. 2018.

[10] D. Piyabongkarn, R. Rajamani, J. A. Grogg, and J. Y. Lew, "Development and experimental evaluation of a slip angle estimator for vehicle stability control," *IEEE Trans. Control Syst. Technol.*, vol. 17, no. 1, pp. 78–88, Jan. 2009.

[11] B. Zhang, H. Du, J. Lam, N. Zhang, and W. Li, "A novel observer design for simultaneous estimation of vehicle steering angle and sideslip angle," *IEEE Trans. Indus. Electron.*, vol. 63, no. 7, pp. 4357–4366, July 2016.

[12] W. Chen, D. Tan, and L. Zhao, "Vehicle sideslip angle and road friction estimation using online gradient descent algorithm," *IEEE Trans. Veh. Technol.*, vol. 67, no. 12, pp. 11 475–11 485, Dec. 2018.

[13] D. M. Bevly, J. C. Gerdes, and C. Wilson, "The use of GPS based velocity measurements for measurement of sideslip and wheel slip," *Veh. Syst. Dyn.*, vol. 38, no. 2, pp. 127–147, 2002.

[14] D. Selmanaj, M. Corno, G. Panzani, and S. M. Savaresi, "Vehicle sideslip estimation: A kinematic based approach," *Control Eng. Pract.*, vol. 67, pp. 1–12, Oct. 2017.

[15] M. Doumiati, A. C. Victorino, A. Charara, and D. Lechner, "Onboard real-time estimation of vehicle lateral tire-road forces and sideslip angle," *IEEE/ASME Trans. Mechatron.*, vol. 16, no. 4, pp. 601–614, Aug. 2011.

[16] K. Nam, S. Oh, H. Fujimoto, and Y. Hori, "Estimation of sideslip and roll angles of electric vehicles using lateral tire force sensors through RLS and Kalman filter approaches," *IEEE Trans. Indus. Electron.*, vol. 60, no. 3, pp. 988–1000, Mar. 2013.

[17] M. Gadola, D. Chindamo, M. Romano, and F. Padula, "Development and validation of a Kalman filter-based model for vehicle slip angle estimation," *Veh. Syst. Dyn.*, vol. 52, no. 1, pp. 68–84, 2014.

[18] H. Du, J. Lam, K.-C. Cheung, W. Li, and N. Zhang, "Sideslip angle estimation and stability control for a vehicle with a non-linear tyre model and a varying speed," *Proc. Inst. Mech. Eng., Part D.*, vol. 229, no. 4, pp. 486–505, Feb. 2015.

[19] A.-T. Nguyen, T.-M. Guerra, and C. Sentouh, "Simultaneous estimation of vehicle lateral dynamics and driver torque using LPV unknown input observer," *IFAC-PapersOnLine*, vol. 51, no. 26, pp. 13–18, Nov. 2018.

[20] X. Li, C. Chan, and Y. Wang, "A reliable fusion methodology for simultaneous estimation of vehicle sideslip and yaw angles," *IEEE Trans. Veh. Technol.*, vol. 65, no. 6, pp. 4440–4458, Jun. 2016.

[21] S. Cheng, L. Li, and J. Chen, "Fusion algorithm design based on adaptive SCKF and integral correction for side-slip angle observation," *IEEE Trans. Indus. Electron.*, vol. 65, no. 7, pp. 5754–5763, July 2018.

[22] L. Imsland, T. A. Johansen, H. F. Grip, and T. I. Fossen, "On non-linear unknown input observers–applied to lateral vehicle velocity estimation on banked roads," *Int. J. Control*, vol. 80, no. 11, pp. 1741–1750, 2007.

[23] G. Phanomchoeng and R. Rajamani, "Real-time estimation of rollover index for tripped rollovers with a novel unknown input nonlinear observer," *IEEE/ASME Trans. Mechatron.*, vol. 19, no. 2, pp. 743–754, Apr. 2014.

[24] D. Ichalal and S. Mammar, "On unknown input observers for LPV systems," *IEEE Trans. Indus. Electron.*, vol. 62, no. 9, pp. 5870–5880, Sept. 2015.

[25] A.-T. Nguyen, C. Sentouh, and J.-C. Popieul, "Driver-automation cooperative approach for shared steering control under multiple system

constraints: Design and experiments," *IEEE Trans. Indus. Electron.*, vol. 64, no. 5, pp. 3819–3830, May 2017.
[26] C. Sentouh, A.-T. Nguyen, M. Benloucif, and J.-C. Popieul, "Driver-automation cooperation oriented approach for shared control of lane keeping assist systems," *IEEE Trans. Control Syst. Technol.*, vol. 27, no. 5, pp. 1962–1978, Sept. 2019.
[27] C. Lv, H. Wang, D. Cao, Y. Zhao, M. Sullman, D. J. Auger, J. Brighton, R. Matthias, L. Skrypchuk, and A. Mouzakitis, "A novel control framework of haptic take-over system for automated vehicles," in *IEEE Intell. Veh. Symp. (IV)*, June 2018, pp. 1596–1601.
[28] K. Yamamoto, D. Koenig, O. Sename, and P. Moulaire, "Driver torque estimation in electric power steering system using an $\mathcal{H}_\infty/\mathcal{H}_2$ proportional integral observer," in *54th IEEE Conf. Decis. Control (CDC)*, Dec. 2015, pp. 843–848.
[29] B. Soualmi, C. Sentouh, and J.-C. Popieul, "Both vehicle state and driver's torque estimation using unknown input proportional multi-integral T-S observer," in *Europ. Control Conf. (ECC)*, June 2014, pp. 2957–2962.
[30] Z. Lendek, J. Lauber, T.-M. Guerra, R. Babuška, and B. De Schutter, "Adaptive observers for TS fuzzy systems with unknown polynomial inputs," *Fuzzy Sets Syst.*, vol. 161, no. 15, pp. 2043–2065, Aug. 2010.
[31] A.-T. Nguyen, T. Taniguchi, L. Eciolaza, V. Campos, R. Palhares, and M. Sugeno, "Fuzzy control systems: Past, present and future," *IEEE Comput. Intell. Mag.*, vol. 14, no. 1, pp. 56–68, Feb. 2019.
[32] M. Chadli and H. Karimi, "Robust observer design for unknown inputs Takagi-Sugeno models," *IEEE Trans. Fuzzy Syst.*, vol. 21, no. 1, pp. 158–164, Feb. 2013.
[33] T. Youssef, M. Chadli, H. R. Karimi, and R. Wang, "Actuator and sensor faults estimation based on proportional integral observer for T-S fuzzy model," *J. Franklin Inst.*, vol. 354, no. 6, pp. 2524–2542, Apr. 2017.
[34] S. Boyd, L. El Ghaoui, E. Feron, and V. Balakrishnan, *Linear Matrix Inequalities in System and Control Theory*. Philadelphia, PA: SIAM, 1994, vol. 15.
[35] A.-T. Nguyen, C. Sentouh, and J.-C. Popieul, "Fuzzy steering control for autonomous vehicles under actuator saturation: Design and experiments," *J. Franklin Inst.*, vol. 355, no. 18, pp. 9374–9395, Dec. 2018.
[36] K. Tanaka and H. Wang, *Fuzzy Control Systems Design and Analysis: a Linear Matrix Inequality Approach*. NY: Wiley-Interscience, 2004.
[37] A.-T. Nguyen, P. Chevrel, and F. Claveau, "LPV static output feedback for constrained direct tilt control of narrow tilting vehicles," *IEEE Trans. Control Syst. Technol.*, pp. 1–10, 2019. [Online]. Available: https://ieeexplore.ieee.org/document/8571182
[38] L. A. Mozelli, R. M. Palhares, F. Souza, and E. M. Mendes, "Reducing conservativeness in recent stability conditions of ts fuzzy systems," *Automatica*, vol. 45, no. 6, pp. 1580–1583, June 2009.
[39] A.-T. Nguyen, P. Chevrel, and F. Claveau, "Gain-scheduled static output feedback control for saturated LPV systems with bounded parameter variations," *Automatica*, vol. 89, pp. 420–424, Mar. 2018.
[40] J.-H. She, X. Xin, and Y. Pan, "Equivalent-input-disturbance approach–Analysis and application to disturbance rejection in dual-stage feed drive control system," *IEEE/ASME Trans. Mechatron.*, vol. 16, no. 2, pp. 330–340, Apr. 2011.
[41] W. Chen, J. Yang, L. Guo, and S. Li, "Disturbance-observer-based control and related methods–An overview," *IEEE Trans. Indus. Electron.*, vol. 63, no. 2, pp. 1083–1095, Feb. 2016.
[42] J. Löfberg, "Yalmip: A toolbox for modeling and optimization in Matlab," in *IEEE Int. Symp. Comput. Aided Control Syst. Des.*, Taipei, Sept. 2004, pp. 284–289.

Anh-Tu Nguyen (M'18) received the degree in engineering and the M.Sc. degree in automatic control from Grenoble Institute of Technology, Grenoble, France, in 2009, and the PhD degree in automatic control from the University of Valenciennes, Valenciennes, France, in 2013.

He is an Associate Professor at the Université Polytechnique Hauts-de-France, and a researcher at the laboratory LAMIH UMR CNRS 8201, Valenciennes, France. His research interests include fuzzy control systems, robust/LPV control and observation, constrained systems, human-machine shared control with strong emphasis on vehicle engineering and robotics applications.

Thierry-Marie Guerra received his PhD degree in automatic control in 1991 from the University of Valenciennes, Valenciennes, France.

He is a Full Professor at the Université Polytechnique Hauts-de-France, Valenciennes, France. He is currently the Head of the Laboratory of Industrial and Human Automation, Mechanics and Computer Science (LAMIH CNRS UMR 8201) (141 researchers and staff, 110 PhD students and post-docs) http://www.univ-valenciennes.fr/LAMIH/. He is chair of the Technical Committee 3.2 "Computational Intelligence in Control" for IFAC, member of the IFAC TC 7.1 "Automotive Control", Area Editor of the international journals: Fuzzy Sets & Systems, IEEE Transactions on Vehicular Technology and IEEE Transactions on Fuzzy Systems. His major research fields and topics of interest are nonlinear control, LPV, quasi-LPV (Takagi-Sugeno) models control and observation, LMI constraints, non-quadratic Lyapunov functions and applications to powertrain systems, disabled persons and soft robotics.

Chouki Sentouh received the M.Sc. degree in automatic control from the University of Versailles, Versailles, France, in 2003, and the PhD degree in automatic control from the University of Évry, Évry, France, in 2007.

He was a postdoctoral researcher at the laboratory IRCCyN UMR CNRS 6597, France, from 2007 to 2009. Since 2009, he is an Associate Professor at the Université Polytechnique Hauts-de-France, laboratory LAMIH UMR CNRS 8201, France. His research fields include automotive control, driver assistance systems with driver interaction, human driver modeling and cooperation in intelligent transportation systems.

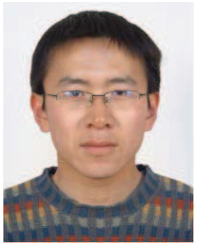

Hui Zhang (M'15, SM'17) received the B.Sc. degree in mechanical design manufacturing and automation from the Harbin Institute of Technology at Weihai, Weihai, China in 2006, the M.Sc. degree in automotive engineering from Jilin University, Changchun, China in 2008, and the Ph.D. degree in mechanical engineering from University of Victoria, Victoria, BC, Canada in 2012.

He was a research associate at the Department of Mechanical and Aerospace Engineering of The Ohio State University, Columbus, Ohio, USA. His research interests include Diesel engine aftertreatment systems, vehicle dynamics and control, mechatronics, robust control and filtering, networked control systems, and signal processing. He is an author/co-author of over 50 peer-reviewed papers on journals and conference proceedings.

Dr. Zhang is a recipient of 2017 IEEE Transactions on Fuzzy Systems Outstanding Paper Award and 2018 SAE Ralph R. Teetor Educational Award. He is a member of SAE International, a senior member of IEEE and a member of ASME. Dr. Zhang has served on the IFAC Technical Committee on Automotive Control, ASME Automotive and Transportation Systems Technical Committee, and SAE Commercial Vehicle Committee. Dr. Zhang serves as an Associate Editor for IEEE Transactions on Vehicular Technology, SAE International Journal of Vehicle Dynamics, Stability, and NVH, SAE International Journal of Connected and Automated Vehicles; Board member of International Journal of Hybrid and Electric Vehicles, Mechanical Systems and Signal Processing; Guest Editor of Mechatronics, IEEE Access, ISA Transactions, Mechanical Systems and Signal Processing, Journal of the Franklin Institute, and International Journal of Vehicle Design; Conference Editorial Board of ASME Dynamic Systems and Control Division, and American Control Conference.